

TRANSPORT OF FINE SANDS BY CURRENTS AND WAVES

By Leo C. Van Rijn,¹ Martin W. C. Nieuwjaar,² Theo van der Kaay,³
Elco Nap,⁴ and Arnold van Kampen⁵

ABSTRACT: The transport process of fine sands in combined current and wave conditions in a flume was studied. Two types of sediment material were used, a very fine sand with a median diameter of about 100 μm and a medium-fine sand with a diameter of 200 μm . The current velocities were varied in the range of 0.1–0.5 m/s (following and opposing the waves). Irregular waves with a single-topped spectrum and peak period of 2.5 s were generated. The significant wave height varied in the range of 0.075 m to 0.18 m. The water depth was about 0.5 m in all tests. Time-averaged fluid velocities were measured by an electromagnetic current meter. Time-averaged sediment concentrations were measured by a pump sampler. The transport rate was obtained by integration of the product of velocity and concentration over the depth. The generation of waves in following or opposing currents causes a decrease of the time-averaged velocities in the near-bed region. A larger wave height results in larger concentrations and in a more uniform distribution over the depth. The influence of the current direction on the concentration profile and the transport rate is negligible.

INTRODUCTION

The knowledge of the suspended sediment transport process in combined current and nonbreaking wave conditions is rather limited. Detailed field data are scarce because of the difficulties in measuring both the fluid velocities and sediment concentrations under wave conditions. Most of the available existing data are related to the longshore sediment transport processes in the surf zone (Jaffe et al. 1984; Osborne and Greenwood 1992). Flume studies of sand transport by waves and currents were mostly related to bed-load transport (Inman and Bowen 1963; Harms 1969; Quick 1983). Inman and Bowen (1963) studied the influence of a very weak current of 0.06 m/s on the bed-load transport process. Transport in and against the wave direction was observed. Sediment suspension was of minor importance. Harms (1969) studied ripple migration and found that the ripples were asymmetric and rounded; the ripple characteristics were strongly related to the relative strength of the wave and current motion. Data on concentrations and transport rates were not given by Harms. Quick (1982) studied the influence of relatively strong currents (± 0.5 m/s) combined with waves on the bed-load transport process. The net transport rate was always

¹Sr. Engr., Delft Hydraulics, P.O. Box 152, Emmeloord, The Netherlands.

²Grad. Student, Coast. Dept. of Tech., Univ. of Delft, P.O. Box 5048, Delft, The Netherlands.

³Grad. Student, Coast. Dept. of Tech., Univ. of Delft, P.O. Box 5048, Delft, The Netherlands.

⁴Grad. Student, Coast. Dept. of Tech., Univ. of Delft, P.O. Box 5048, Delft, The Netherlands.

⁵Grad. Student, Coast. Dept. of Tech., Univ. of Delft, P.O. Box 5048, Delft, The Netherlands.

Note. Discussion open until August 1, 1993. To extend the closing date one month, a written request must be filed with the ASCE Manager of Journals. The manuscript for this paper was submitted for review and possible publication on October 17, 1991. This paper is part of the *Journal of Waterway, Port, Coastal, and Ocean Engineering*, Vol. 119, No. 2, March/April, 1993. ©ASCE, ISSN 0733-950X/93/0002-0123/\$1.00 + \$.15 per page. Paper No. 2644.

in the direction of the wave propagation as long as the opposing current was not larger than 0.2 m/s.

Bosman (1982) and Bosman and Steetzel (1986) studied the effect of currents combined with waves on the suspended load transport over a sloping bed of 100 μm sand (nonuniform conditions). An extension of their experimental results is presented in this study, which is a part of a long-term experimental research of (fine) sand transport in combined currents and waves started in 1987 as a joint effort of Delft University of Technology and Delft Hydraulics. This research program was also sponsored by the MAST-program of the European Communities and by the Rijkswaterstaat of the Dutch Ministry of Public Works. The main objective of this research program is the systematic study of the suspended sediment transport process under currents and nonbreaking waves both in a flume and in a basin. In the present paper, the suspended sediment transport process of fine sands in currents (following and opposing) superimposed by nonbreaking waves in a flume is studied.

The instantaneous suspended sediment transport rate can be computed from the product of the instantaneous velocities and concentrations defined as $U_z(x, t) = u_z + \bar{u}_z(x, t)$ and $C_z(x, t) = c_z + \bar{c}_z(x, t)$ with \bar{u}_z, \bar{c}_z being the fluctuating components at a certain elevation above the bed and $u_z = 1/L1/T \iint U_z dx dt$ and $c_z = 1/L1/T \iint C_z dx dt$ being the time and space-averaged velocity and concentration at the same elevation above the bed (L is the average bed form length and T is the wave period). Space averaging over length L must be applied to eliminate the strong influence of the bed forms on the local variables (Bosman and Steetzel 1986). The instantaneous transport rate Q is defined as

$$Q_{x,t} = \int_a^{h+\eta} U_z C_z dz$$

$$= \int_a^{h+\eta} [u_z c_z + u_z \bar{c}_z + \bar{u}_z c_z + \bar{u}_z \bar{c}_z] dz \dots\dots\dots (1)$$

with h = water depth; η = water surface elevation; and a = bed boundary level.

Averaging over a longitudinal distance of several bed form lengths (indicated by $\langle \rangle$) and over time (indicated by an overbar) and assuming relatively small waves ($\eta \ll h$) and relatively small sediment concentrations near the water surface, the time- and space-averaged suspended transport rate q_s can be represented as

$$q_s = \langle Q \rangle = \int_a^h [\langle \overline{u_z c_z} \rangle + \langle \overline{u_z \bar{c}_z} \rangle + \langle \overline{\bar{u}_z c_z} \rangle + \langle \overline{\bar{u}_z \bar{c}_z} \rangle] dz$$

$$= \int_a^h [u_z c_z + u_z \langle \bar{c}_z \rangle + \langle \bar{u}_z \rangle c_z + \langle \overline{\bar{u}_z \bar{c}_z} \rangle] dz \dots\dots\dots (2)$$

By definition $\langle \bar{c}_z \rangle = 0$ and $\langle \bar{u}_z \rangle = 0$, giving

$$q_s = \int_a^h u_z c_z dz + \int_a^h \langle \overline{\bar{u}_z \bar{c}_z} \rangle dz \dots\dots\dots (3)$$

The first term on the right-hand side of (3) represents the steady current-related suspended transport component $q_{s,c}$, which can be determined by measuring the vertical distribution of the time- and space-averaged velocities

and concentrations. The second term represents the transport by the fluctuating components due to turbulence and waves. Since the orbital velocities are much larger than the turbulent velocities, the second term on the right-hand side of (3) is termed the wave-related suspended transport component $q_{s,w}$. Thus, $q_s = q_{s,c} + q_{s,w}$. The total sediment transport rate q_t can be obtained by adding the current-related bed-load transport rate $q_{b,c}$ and the wave-related bed-load transport rate $q_{b,w}$. Thus, $q_t = (q_{s,c} + q_{b,c}) + (q_{s,w} + q_{b,w}) = q_{t,c} + q_{t,w}$.

In the present study, attention is focussed primarily on the current-related suspended transport rate $q_{s,c}$ for two types of bed material ($d_{50} = 100$ and $200 \mu\text{m}$). In some tests the total wave-related transport component $q_{t,w}$ was also measured.

The experimental results have been used to determine the influence of wave height, current velocity, and sediment size on the current-related transport rate. The results have also been used to verify the predictive capability of the sediment transport models of Bijker (1971), Nielsen (1985), and Van Rijn (1985, 1989).

EXPERIMENTAL SETUP

The experiments were conducted in a flume of the Laboratory of Fluid Mechanics of the Civil Engineering Department of the Delft University, The Netherlands. The flume has a total length of approximately 45 m, a width of 0.8 m, and a depth of 1.0 m. Irregular waves (single-topped spectrum) were generated in combination with following or opposing currents. The current was generated by a constant-head system in the laboratory. In the flume, a horizontal sand bed (length 25 m, thickness 0.1 m) was installed. The water was recirculated through a settling basin where most of the sediment load was trapped.

The direction of the current was established by manipulation of gate valves and the use of (temporary) weirs. By adjusting the height of the weir at the end of the flume, the desired water depth (0.5 m) was obtained. A wave damping structure was present at the end of the flume.

The water entering the flume had no initial sediment load. Consequently, the concentration profiles were generated by erosion of sediment particles in the section with the sand bed. To provide enough length for establishing equilibrium concentrations, the measuring section was situated at a distance of approximately thirty times the water depth from the beginning of the bed.

Two types of sediment material were used: a very fine sand of about $100 \mu\text{m}$ ($d_{10} = 80 \mu\text{m}$, $d_{50} = 105 \mu\text{m}$, $d_{90} = 150 \mu\text{m}$) and a fine sand of about $200 \mu\text{m}$ ($d_{10} = 150 \mu\text{m}$, $d_{50} = 205 \mu\text{m}$, $d_{90} = 295 \mu\text{m}$). Before the sand was brought into the flume, the silt particles were washed out while pebbles and shells were removed by sieving (3 mm sieve). During the experiments, little variation in particle size was observed at the measuring location.

Water-level variations were measured with a resistance probe near the location where the concentrations and velocities were measured. The measuring period was chosen to be 30 min. Assuming Rayleigh-distributed wave heights, the characteristic wave parameters were computed from the wave spectrum, as follows: $H_s = 4(m_0)^{0.5}$; $T_z = (m_0/m_2)^{0.5}$; and $T_p = 1/f_p$, in which: H_s = significant wave height; T_z = zero-crossing period; T_p = wave spectrum peak period; f_p = wave spectrum peak frequency; and m_n = n th order moment of wave spectrum.

The characteristic amplitudes of the orbital horizontal velocity \hat{U}_s and

the displacement \hat{A}_8 just outside the wave boundary layer were computed using linear wave theory. Significant wave height was used for the characteristic wave height and the wave spectrum peak period for the characteristic wave period. To account for the presence of the current, the relative peak period and the corresponding wave length were used in the wave formulas (Jonsson et al. 1970).

Sediment concentrations were determined from water-sediment samples using a pump sampling instrument. This instrument consisted of an array of ten intake tubes of 3 mm internal diameter connected to the pumps by plastic hoses. The lowest intake tube was placed at about 0.01 m above the crest level of the bed forms. The intake openings were placed transverse to the plane of orbital motion. This arrangement yields a trapping ratio (measured concentration divided by true concentration) less than unity because the sediment particles cannot always follow the curved fluid paths into the intake tubes. The concentrations were corrected for this effect (Bosman et al. 1987). The intake velocity was about 1.4 m/s, satisfying sampling requirements. The 10 L samples (sampling period of 20 min) were collected in calibrated buckets.

The fluid velocities were measured using an electromagnetic velocity meter with a measuring volume of about $3 \times 3 \times 3 \text{ mm}^3$ below the probe. The velocities were measured at the same elevations above the mean bed as those of the concentrations starting at the lowest point and working upwards. A time-averaging period of 256 s (approx. 100 waves) was applied, which gave reproducible results as shown by preliminary tests.

Space averaging over the bed form length was performed by movement of the sediment concentration and fluid velocity instruments forward and backward over a certain longitudinal distance by use of an oscillating carriage on top of the flume. The velocity of the moving carriage (approx. 0.01 m/s) was small compared with the fluid velocity and large compared with the bed-form migration velocity. The error in the time-averaged velocity was less than 0.00125 m/s in the present tests. Preliminary tests showed that a space-averaging distance of 0.6 m (approx. 5 ripple lengths) was sufficiently large to give reproducible results (inaccuracy of about 30%).

The mean bed level at the measuring section was determined using an electronic profile follower and a signal integrator in three longitudinal sections before and after each test.

Based on these results, the distance between the lowest measuring point (velocity and concentration) and the mean bed level was determined in each test.

The applied test program is given in Tables 1 and 2. The test code refers to the approximate sediment size, wave height, and current velocity. For example, T100,10,-40 represents an experiment with a mean sediment size of 100 μm , a wave height of approximately 10 cm, and a current velocity of approximately 40 cm/s against (negative sign) the wave direction. All experiments were performed in a water depth of approximately 0.5 m. Detailed velocity and concentration data are presented by Van der Kaaij and Nieuwjaar (1987) and by Nap and Van Kampen (1988).

EXPERIMENTAL RESULTS

Time and Bed-Averaged Concentrations

Fig. 1 shows the influence of wave height on the concentration profiles for the 200 μm sediment. An increase of the wave height yields: (1) An increase of the sediment concentrations which is relatively large in case of

TABLE 1. Basic Hydraulic Data for 100 μm Sediment

Test number (1)	Water depth h (m) (2)	Wave height H_s (m) (3)	Peak period T_p (s) (4)	Current velocity \bar{u} (m/s) (5)	Sediment size d_{50} (μm) (6)	Ripple height Δ_r (m) (7)	Ripple length λ_r (m) (8)	Current-related bed-load transport rate $q_{b,c}$ (kg/sm) (9)	Current-related suspended-load transport rate $q_{s,c}$ (kg/sm) (10)
T100,7.5,10	0.510	0.073	2.3	0.101	108	0.010	0.066	$1.0 \cdot 10^{-5}$	$2.6 \cdot 10^{-4}$
T100,7.5,-10	0.480	0.071	2.3	-0.094	100	0.010	0.063	$-1.0 \cdot 10^{-5}$	$-3.6 \cdot 10^{-4}$
T100,7.5,20	0.510	0.075	2.3	0.191	106	0.013	0.084	$4.0 \cdot 10^{-5}$	$1.8 \cdot 10^{-3}$
T100,7.5,-20	0.490	0.071	2.2	-0.184	111	0.009	0.068	$-2.0 \cdot 10^{-5}$	$-3.0 \cdot 10^{-3}$
T100,7.5,40	0.520	0.077	2.3	0.364	108	0.012	0.094	$1.5 \cdot 10^{-3}$	$3.3 \cdot 10^{-2}$
T100,7.5,-40	0.490	0.072	2.4	-0.390	112	0.015	0.089	$-1.1 \cdot 10^{-3}$	$-3.2 \cdot 10^{-2}$
T100,10,10	0.500	0.104	2.3	0.100	107	0.010	0.066	$5.0 \cdot 10^{-5}$	$1.1 \cdot 10^{-3}$
T100,10,-10	0.500	0.101	2.3	-0.106	110	0.008	0.060	$-1.0 \cdot 10^{-5}$	$-1.6 \cdot 10^{-3}$
T100,10,20	0.490	0.101	2.3	0.200	100	0.012	0.081	$1.7 \cdot 10^{-4}$	$7.5 \cdot 10^{-3}$
T100,10,-20	0.490	0.105	2.3	-0.200	111	0.009	0.063	$-1.2 \cdot 10^{-4}$	$-6.9 \cdot 10^{-3}$
T100,10,40	0.500	0.095	2.3	0.350	109	0.014	0.111	$1.5 \cdot 10^{-3}$	$4.8 \cdot 10^{-2}$
T100,10,-40	0.490	0.103	2.5	-0.390	113	0.014	0.110	$-2.3 \cdot 10^{-3}$	$-5.0 \cdot 10^{-2}$
T100,15,10	0.490	0.147	2.6	0.092	107	0.009	0.065	$6.0 \cdot 10^{-5}$	$2.3 \cdot 10^{-3}$
T100,15,-10	0.490	0.148	2.3	-0.120	110	0.008	0.062	$-1.4 \cdot 10^{-4}$	$-5.3 \cdot 10^{-3}$
T100,15,20	0.504	0.149	2.6	0.193	109	0.011	0.078	$4.0 \cdot 10^{-4}$	$1.1 \cdot 10^{-2}$
T100,15,-20	0.494	0.148	2.3	-0.210	112	0.006	0.063	$-1.6 \cdot 10^{-4}$	$-1.4 \cdot 10^{-2}$
T100,15,40	0.505	0.140	2.3	0.386	105	0.015	0.118	$2.8 \cdot 10^{-3}$	$9.7 \cdot 10^{-2}$
T100,15,-40	0.504	0.141	2.7	-0.380	113	0.019	0.145	$-6.2 \cdot 10^{-3}$	$-8.1 \cdot 10^{-2}$
T100,18,10	0.496	0.180	2.6	0.090	105	0.009	0.067	$1.1 \cdot 10^{-4}$	$4.0 \cdot 10^{-3}$
T100,18,-10	0.494	0.180	2.3	-0.131	111	0.007	0.068	$-1.6 \cdot 10^{-4}$	$-7.2 \cdot 10^{-3}$
T100,18,20	0.510	0.180	2.6	0.183	111	0.011	0.079	$4.5 \cdot 10^{-4}$	$1.2 \cdot 10^{-2}$
T100,18,-20	0.486	0.180	2.3	-0.210	112	0.007	0.060	$-3.9 \cdot 10^{-4}$	$-1.9 \cdot 10^{-2}$
T100,18,-40	0.500	0.177	2.5	-0.400	111	0.015	0.114	$-2.6 \cdot 10^{-3}$	$-9.3 \cdot 10^{-2}$

TABLE 2. Basic Hydraulic Data for 200 μm Sediment

Test number (1)	Water depth h (m) (2)	Wave height H_s (m) (3)	Peak period T_p (s) (4)	Current velocity u (m/s) (5)	Sediment size d_{50} (μm) (6)	Ripple height Δ_r (m) (7)	Ripple length λ_r (m) (8)	Current-related bed-load transport rate $q_{b,c}$ (kg/sm) (9)	Current-related suspended-load transport rate $q_{s,c}$ (kg/sm) (10)
T200,7.5,10	0.51	0.076	2.6	0.11	200	0.016	0.093	$4.1 \cdot 10^{-6}$	$2.3 \cdot 10^{-5}$
T200,7.5,20	0.51	0.074	2.4	0.23	203	0.015	0.099	$1.9 \cdot 10^{-4}$	$2.1 \cdot 10^{-4}$
T200,7.5,40	0.50	0.076	2.4	0.45	203	0.014	0.134	$1.6 \cdot 10^{-3}$	$1.1 \cdot 10^{-2}$
T200,10,10	0.52	0.106	2.6	0.12	205	0.017	0.092	$6.2 \cdot 10^{-5}$	$8.6 \cdot 10^{-5}$
T200,10,-10	0.49	0.098	2.5	-0.13	209	0.013	0.089	$3.3 \cdot 10^{-5}$	$-1.5 \cdot 10^{-4}$
T200,10,20	0.51	0.099	2.5	0.22	212	0.017	0.099	$2.4 \cdot 10^{-4}$	$9.5 \cdot 10^{-4}$
T200,10,-20	0.49	0.096	2.5	-0.22	209	0.019	0.114	$-1.3 \cdot 10^{-4}$	$-7.8 \cdot 10^{-4}$
T200,10,40	0.51	0.098	2.6	0.45	205	0.019	0.153	$2.8 \cdot 10^{-3}$	$2.1 \cdot 10^{-2}$
T200,10,-40	0.50	0.101	2.5	-0.45	206	0.021	0.156	$-3.7 \cdot 10^{-3}$	$-2.5 \cdot 10^{-2}$
T200,12,10	0.52	0.121	2.5	0.10	208	0.016	0.100	$1.9 \cdot 10^{-4}$	$3.7 \cdot 10^{-4}$
T200,12,-10	0.50	0.115	2.5	-0.12	212	0.016	0.102	$3.4 \cdot 10^{-5}$	$-2.6 \cdot 10^{-4}$
T200,12,20	0.51	0.123	2.6	0.22	203	0.017	0.108	$3.5 \cdot 10^{-4}$	$1.7 \cdot 10^{-3}$
T200,12,-20	0.49	0.116	2.5	-0.23	206	0.018	0.111	$-1.7 \cdot 10^{-4}$	$-1.6 \cdot 10^{-3}$
T200,12,40	0.51	0.119	2.5	0.44	204	0.018	0.174	$5.2 \cdot 10^{-3}$	$2.5 \cdot 10^{-2}$
T200,12,-40	0.50	0.118	2.6	-0.44	200	0.020	0.155	$-3.6 \cdot 10^{-3}$	$2.9 \cdot 10^{-2}$
T200,15,10	0.50	0.146	2.4	0.11	218	0.018	0.100	$1.2 \cdot 10^{-4}$	$7.3 \cdot 10^{-4}$
T200,15,-10	0.50	0.149	2.5	-0.13	223	0.017	0.109	$8.1 \cdot 10^{-5}$	$-1.0 \cdot 10^{-3}$
T200,15,20	0.51	0.151	2.4	0.22	211	0.016	0.111	$6.7 \cdot 10^{-4}$	$4.5 \cdot 10^{-3}$
T200,15,-20	0.49	0.147	2.5	-0.23	205	0.013	0.092	$-1.0 \cdot 10^{-4}$	$-3.1 \cdot 10^{-3}$
T200,15,-40	0.51	0.146	2.5	-0.44	200	0.024	0.188	$-8.3 \cdot 10^{-3}$	$-4.0 \cdot 10^{-2}$
T200,17.5,-20	0.50	0.177	2.5	-0.23	205	0.013	0.095	$-4.6 \cdot 10^{-4}$	$-3.7 \cdot 10^{-3}$
T200,18.5,-40	0.52	0.186	2.4	-0.43	211	0.029	0.200	$-8.5 \cdot 10^{-3}$	$-6.0 \cdot 10^{-2}$

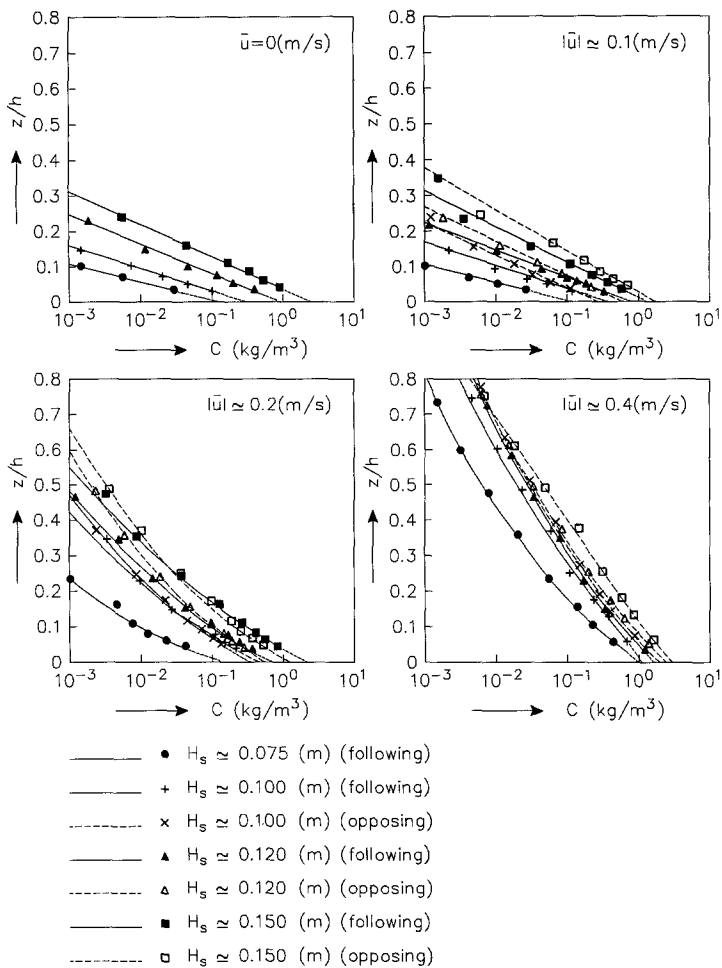


FIG. 1. Influence of Wave Height on Concentration Profile for 200 μm Sediment

a weak current $\bar{u} = 0.1$ and 0.2 m/s, and relatively small in case of a strong current of $\bar{u} = 0.4$ m/s, (2) an increase of the steepness of the concentration profile as a result an increased wave-induced mixing (larger orbital velocities and larger ripple heights). Similar results have been obtained for the experiments with the $100 \mu\text{m}$ sediment. It is noted that the sediment concentrations in the upper layers of the depth at the current velocities of 0.4 m/s are somewhat too small (about 30%), because the flume was not long enough for establishing equilibrium concentrations in the upper half of the flow depth.

Fig. 2 shows the influence of the current velocity on the concentrations. A weak current of 0.1 m/s superimposed on the waves negligibly influences the magnitude of the concentrations. A stronger current of 0.2 m/s increases the concentrations in the upper layer due to increased mixing effects, while those in the near-bed region remain approximately constant. A relatively strong current of 0.4 m/s increases the concentrations over the entire profile.

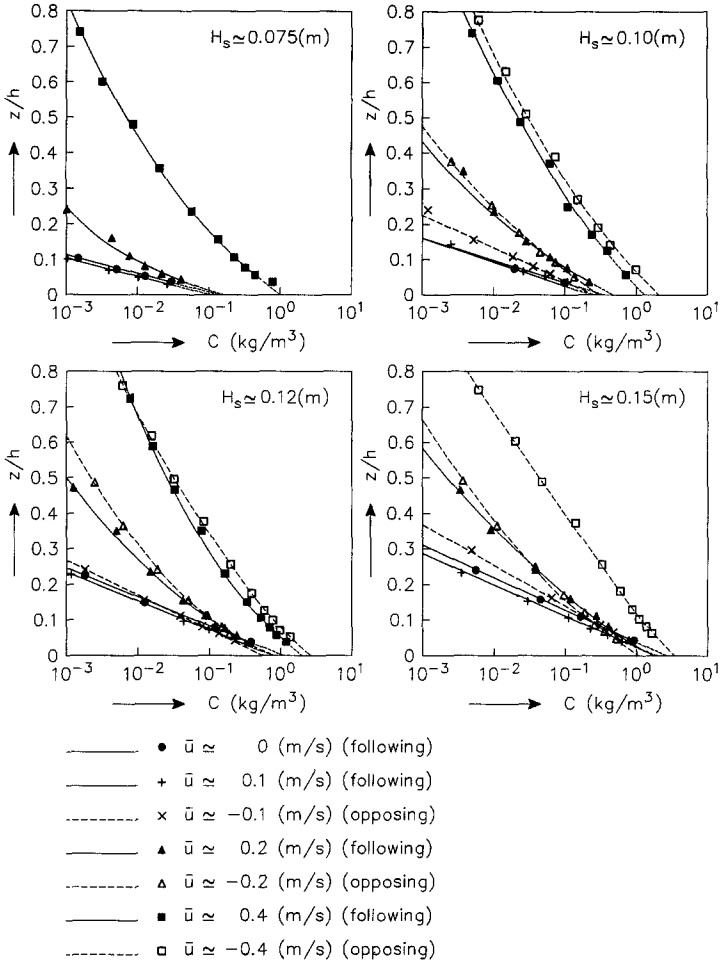


FIG. 2. Influence of Current Velocity on Concentration Profile for 200 μm Sediment

The current direction has a minor effect on the concentration profiles. Comparison of near-bed concentrations (at the same wave height and current velocity) for a different current direction shows maximum differences of about 30%. In case of an opposing current the concentrations in the upper layers are slightly larger, as shown by the broken curves in Fig. 2. This may be caused by an increased upward mixing due to the presence of larger velocity gradients, which are generated in opposing currents. This trend was also observed with the 100 μm sediment.

When a very weak current ($|\bar{u}| = 0.1$ m/s) or no current is superimposed on the waves, the measured concentration profiles can be presented by the following distribution:

$$c_z = c_b \exp\left(\frac{-z}{L_c}\right) \dots \dots \dots (4)$$

in which c_z = time- and bed-averaged concentration at height z ; c_b = reference concentration at $z = 0$; and L_c = vertical length scale (order ripple height).

Eq. (4) cannot be used when a stronger current ($|\bar{u}| = 0.2, 0.4$ m/s) is superimposed on the waves. For increasing current velocities the current-induced mixing becomes more important, resulting in larger sediment concentrations in the upper layers.

Time- and Bed-Averaged Fluid Velocities

Measured velocity profiles show a clear influence of the waves in both experiments (100 μm and 200 μm sediment). Fig. 3 shows measured current velocity profiles of following currents for the 200 μm experiments. The velocities are made dimensionless with the depth-averaged velocity \bar{u} . For comparison, the current velocity profile measured over the same rippled bed without waves (after stopping the wave generator) is also shown. In the tests with $\bar{u} = \pm 0.1$ m/s and ± 0.2 m/s, the presence of waves causes a decrease of the velocities in the near-bed layer ($z/h < 0.2$) and in the near-surface layer ($z/h > 0.6$) and an increase of the velocities in the intermediate layer. These deviations are most pronounced when the peak value of the near-bed orbital velocity (U_b) is relatively large compared to the depth-averaged velocity (\bar{u}).

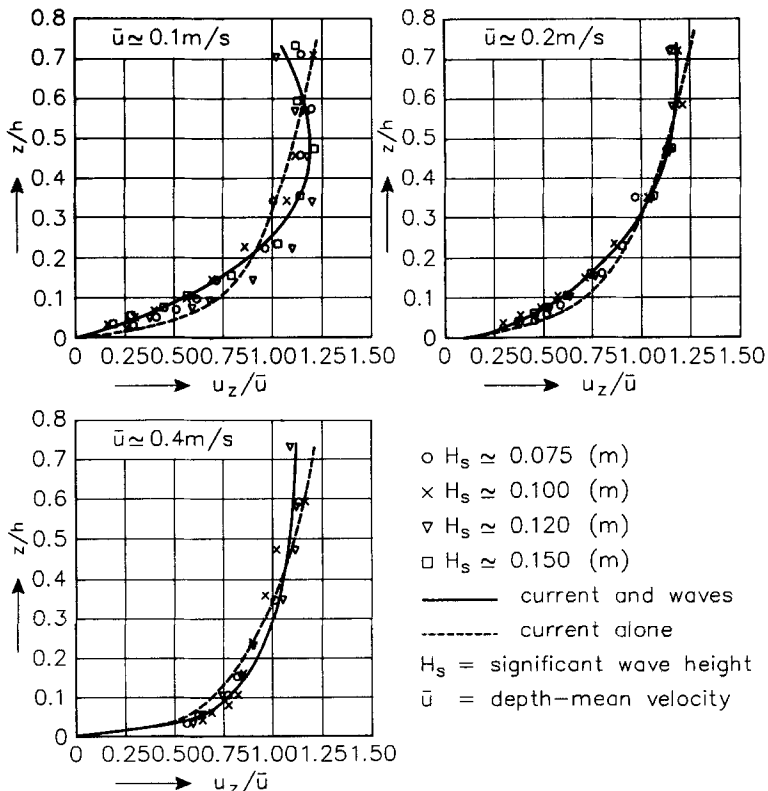


FIG. 3. Influence of Waves on Current Velocity Profile: Following Current

Fig. 4 shows the current velocity profiles of opposing currents for the 200 μm experiment. The presence of waves causes a decrease of the current velocities in the near-bed region ($z/h < 0.2$), which is significantly larger than in the case of following currents, and an increase of the velocities in upper layer ($z/h > 0.5$). These deviations are most pronounced with relatively large waves combined with a weak opposing current ($\bar{u} = -0.1$ m/s). Similar effects for opposing and following currents were observed by Kemp and Simons (1982, 1983) for a plane bed.

Ripple and Roughness Characteristics

Two-dimensional ripples were observed for relatively small waves without a current. The ripples became three-dimensional with increasing wave height and current velocity. The ripples were symmetrical with waves alone and asymmetrical when a current was superimposed on the waves. The overall ripple dimensions are given in Tables 1 and 2. The near-bed velocities measured in a current alone (after stopping the wave generator) were analyzed by fitting a logarithmic distribution to the measured velocities to determine the physical bed roughness height k_s (Van Rijn 1990). The k_s values were found to be on the order of 3–7 times the ripple height. A clear influence of the ripple steepness ($= 0.1$ to 0.2) could not be detected.

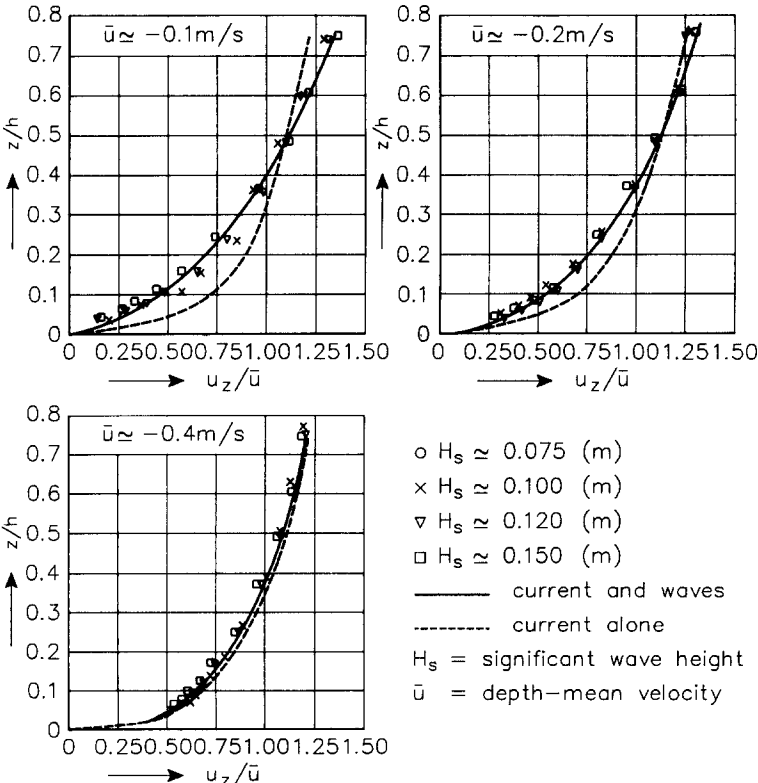


FIG. 4. Influence of Waves on Current Velocity Profile: Opposing Current

Current-Related Sediment Transport

The total current-related sediment transport rate $q_{t,c}$ passing a section was determined as the sum of the current-related suspended-load transport $q_{s,c}$ and the current-related bed-load transport $q_{b,c}$. Thus $q_{t,c} = q_{s,c} + q_{b,c}$.

The current-related bed-load transport rate was estimated from the measured bed-form characteristics, as follows:

$$q_{b,c} = 0.6\rho_s(1 - p)v_r\Delta_r \dots\dots\dots (5)$$

in which ρ_s = sediment density = 2,650 kg/m³; p = porosity factor of bed material = 0.4; v_r = ripple migration velocity; and Δ_r = ripple height.

The measured $q_{b,c}$ values are presented in Tables 1 and 2. The inaccuracy of these values may be rather large, because only a few ripples were studied close to the flume window.

The current-related suspended-load transport is defined as the integration of the product of the time- and space-averaged concentrations c_z and velocities u_z from the bed-form crest to the water surface (see Fig. 5). Thus:

$$q_{s,c} = \int_{1/2\Delta_r}^h u_z c_z dz \dots\dots\dots (6)$$

To estimate the local-transport rate in the unmeasured regions between the lowest measuring point and the ripple crest and between the highest measuring point and the water surface (see Fig. 5), the following methods were applied:

- The concentrations between the lowest measuring point and the ripple crest are represented by an exponential function $c_z = \exp(Az + B)$. The A and B coefficients were obtained by fitting of this latter equation to the concentrations in the lowest three measuring points.
- The fluid velocities between the lowest measuring point and the ripple crest level are represented by the following exponential function: $u_z = u_1(z/z_1)^{0.25}$ in which u_1 = fluid velocity measured in the lowest measuring point z_1 .
- The concentrations between the highest measuring point and the

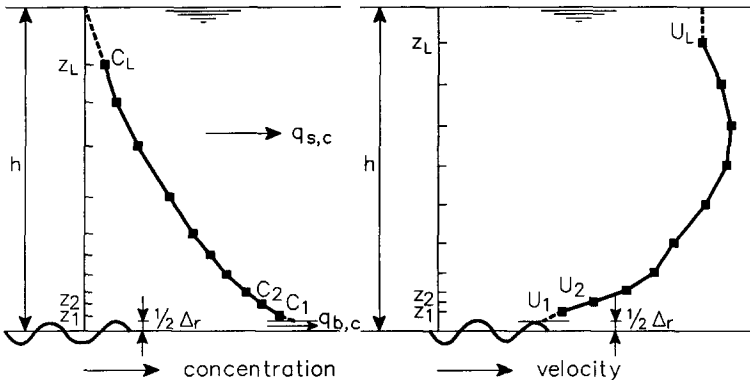


FIG. 5. Extrapolation of Measured Concentration and Velocity Profiles

water surface are represented by a linear function giving a concentration equal to zero at the water surface.

- The fluid velocities between the highest measuring point and the water surface are assumed to be constant and equal to the fluid velocity in the highest measuring point.

The first assumption is the most crucial because it is related to the extrapolation of the concentrations in a region with large gradients, which may result in considerable errors. Therefore, other distributions were applied in preliminary computations giving variations of the transport rates of about 30%. This latter value is supposed to be the inaccuracy of the measured current-related suspended-load transport rates.

The transport rates based on the aforementioned method are reported in Table 1. Analysis of the measured current-related transport rates showed almost no influence of the wave direction on the transport rates. Fig. 6 shows the current-related transport $q_{t,c}$ as a function of the significant wave height for different velocities. Fig. 7 shows the influence of the current velocity for different wave heights. In both graphs, the data points have been omitted for clearness. The following phenomena can be observed:

- Relatively large increase of the transport rate with increasing wave height ($q_{t,c} \approx H_s^5$) when a weak current ($\bar{u} = 0.1$ m/s) is present.
- Relatively small increase of the transport rate with increasing wave height ($q_{t,c} \approx H_s^2$) when a strong current ($\bar{u} = 0.4$ m/s) is present.
- Relatively large increase of the transport rate with increasing depth-averaged velocity [$q_{t,c} \approx (\bar{u})^{4.0}$] when low waves ($H_s/h = 0.15$) are present.
- Relatively small increase of the transport rate with increasing depth-averaged velocity [$q_{t,c} \approx (\bar{u})^{2.5}$] when high waves ($H_s/h = 0.35$) are present.

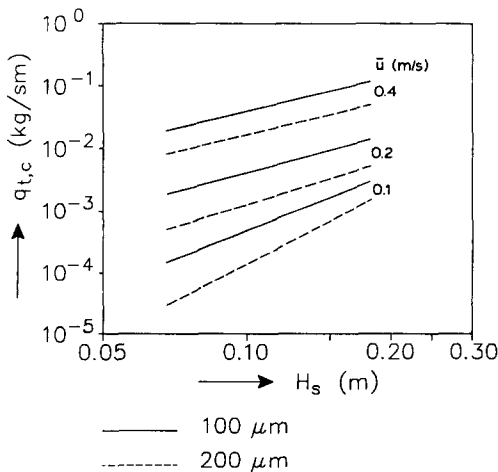


FIG. 6. Current-Related Transport Rate as Function of Wave Height for Different Current Velocities

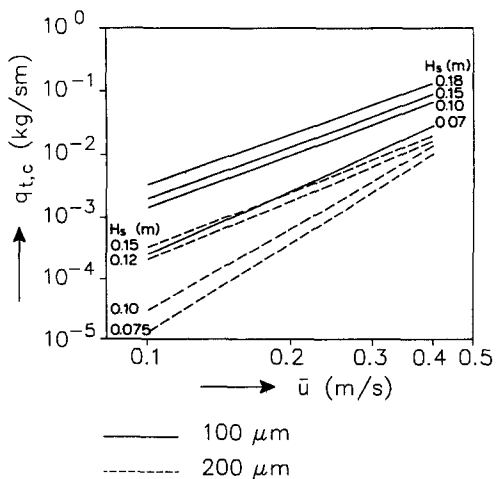


FIG. 7. Current-Related Transport Rate as Function of Current Velocity for Different Wave Heights

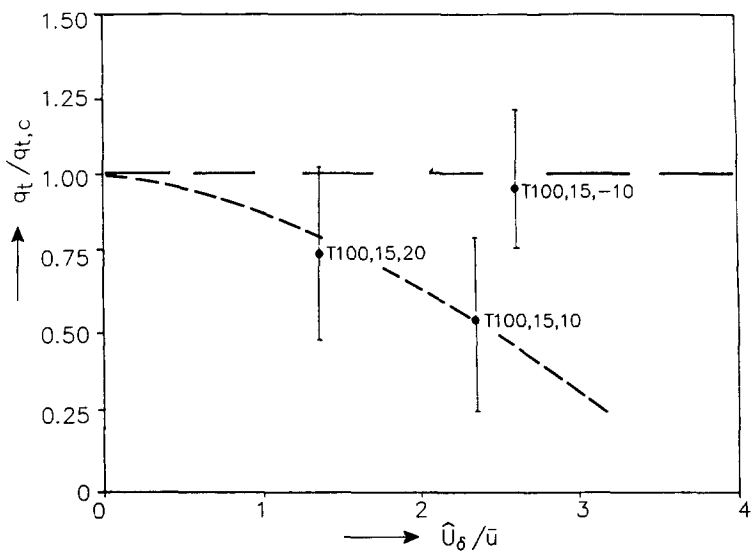


FIG. 8. Ratio of Total Transport and Total Current-Related Transport (100 μm Sediment)

- A decrease of the transport rate by a factor 3 to 6 due to an increase of the sediment size by a factor 2 (from 100 μm to 200 μm).

The results show a relatively small sensitivity of the current velocity and the wave height on the transport rates in case of a strong current and/or high waves.

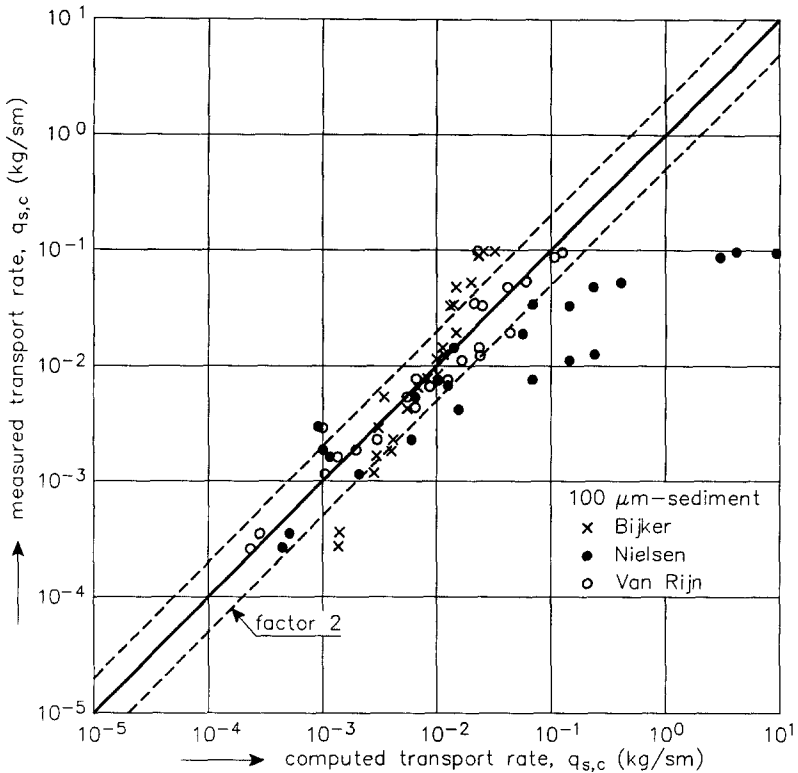


FIG. 9. Measured and Computed Transport Rates for 100 μm Sediment

Wave-Related Sediment Transport

To obtain quantitative information of the relative importance of the total wave-related transport rate ($q_{t,w}$) with respect to the total current-related transport ($q_{t,c}$), special sand balance tests were performed. These tests consisted of measuring the sediment mass eroded from the bed between the flume entrance and a section S at a distance of 15 m from the entrance. Since there was no sediment feed at the flume entrance, the total time-averaged transport rate q_t passing the section S is equal to the eroded mass divided by the elapsed time period. The eroded mass was obtained by weighing (underwater) the bed material mass before and after the tests.

Time- and space-averaged velocity and concentration profiles and bed-form characteristics were simultaneously obtained at section S to determine the total current-related transport $q_{t,c} = q_{s,c} + q_{b,c}$; see (5) and (6).

Three experiments with the 100 μm sediment were performed: two experiments with a following current of about 0.1 m/s and 0.2 m/s ($T_{100,15,10}$ and $T_{100,15,20}$), and one experiment with an opposing current of about 0.1 m/s ($T_{100,15,-10}$). The significant wave height was about 0.15 m in all three tests. The experimental results are presented in Fig. 8 showing the ratio of the total transport rate q_t and the total current-related transport rate $q_{t,c}$ as a function of the ratio U_s/\bar{u} . The most important results are:

- The total transport rate $q_t = q_{t,w} + q_{t,c}$ is smaller than the total

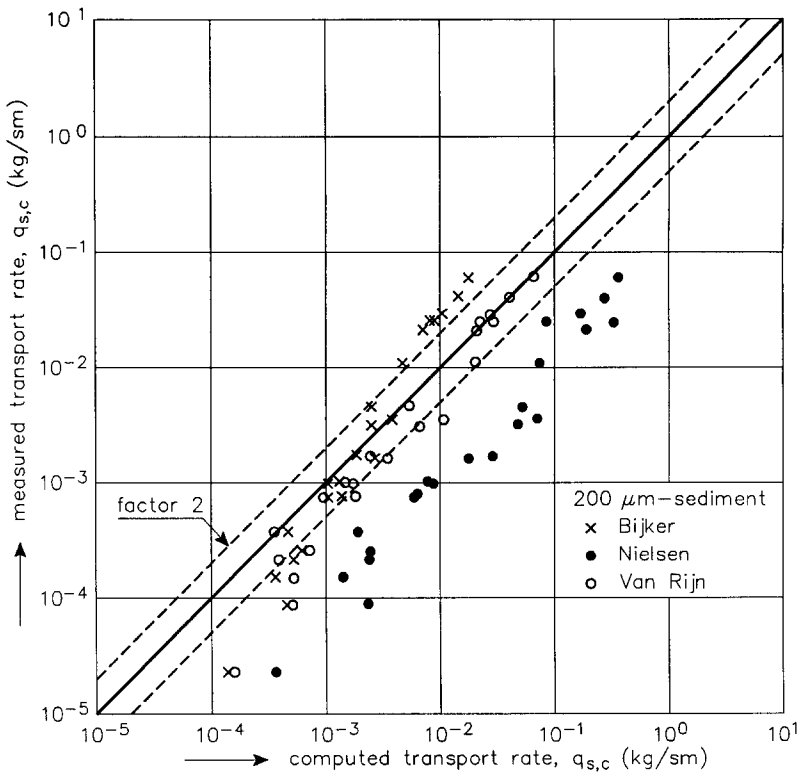


FIG. 10. Measured and Computed Transport Rates for 200 μm Sediment

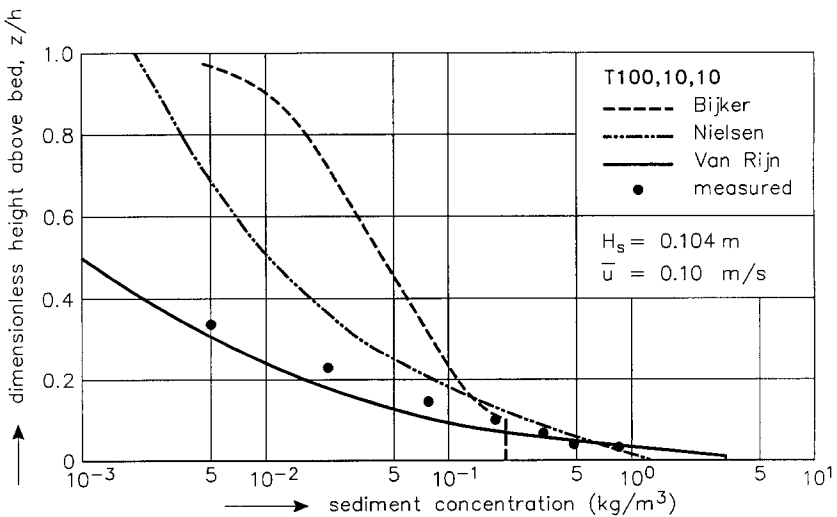


FIG. 11. Measured and Computed Concentration Profiles (T100,10,10)

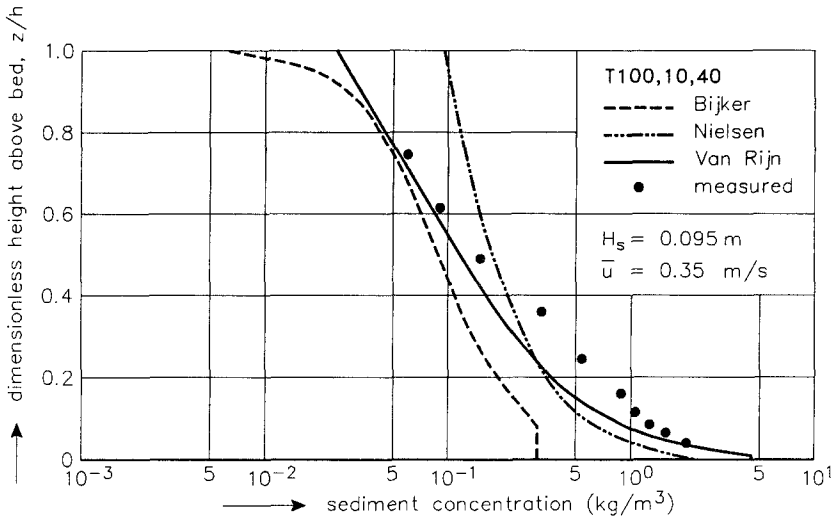


FIG. 12. Measured and Computed Concentration Profiles (T100,10,40)

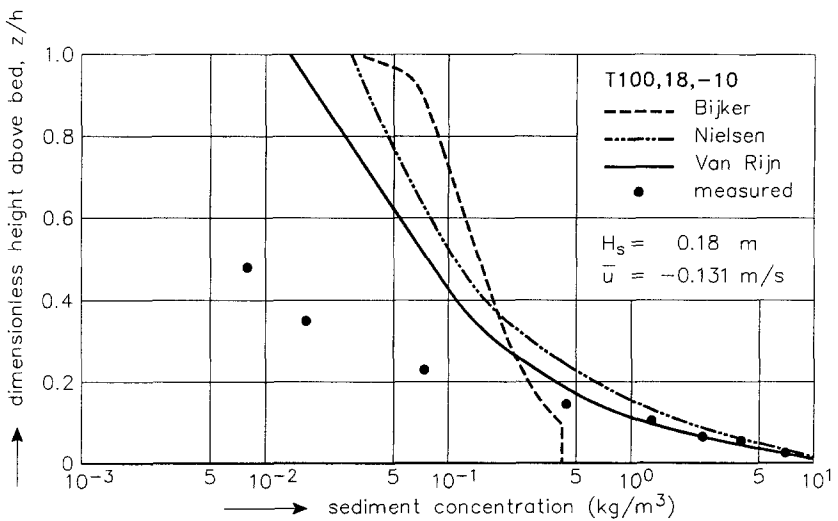


FIG. 13. Measured and Computed Concentration Profiles (T100,18,-10)

current-related transport rate $q_{t,c}$ for a following current, which means that the wave-related transport $q_{t,w}$ is directed against the wave and current direction.

- The wave-related transport is largest for a weak following current (T100,15,10).
- The wave-related transport seems to be negligible in case of an opposing current (T100,15,-10).

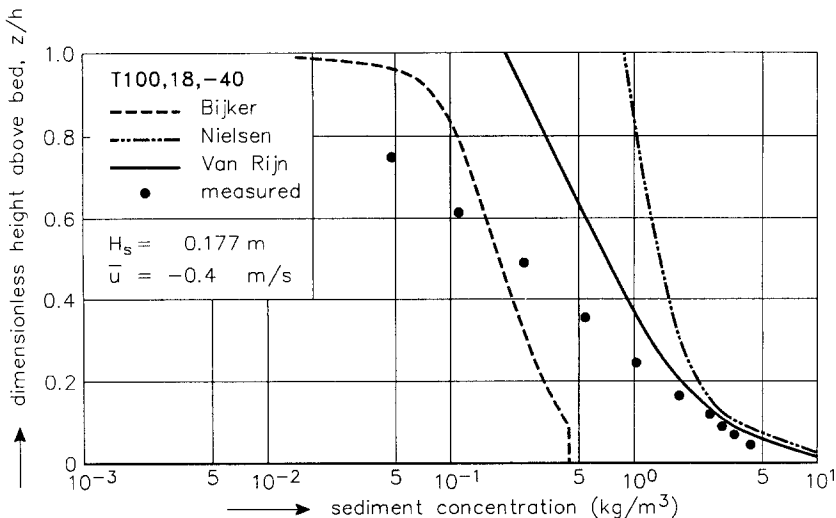


FIG. 14. Measured and Computed Concentration Profiles (T100,18,-40)

The underlying mechanism of (wave-related) transport processes against the wave direction is strongly related to the near-bed eddy motions.

When the wave crest (superimposed on a following current) passes a ripple, the near-bed velocities will be relatively large and a strong eddy with high sand concentrations is generated at the ripple back. When the wave trough passes the ripple, the eddy is lifted and carried against the wave propagation direction. After that, the eddy disintegrates at higher levels. Some of the sediment particles will fall back to the bed during this process. Simultaneously, another eddy is generated at the ripple front when the wave trough passes. During this phase of the wave cycle, the near-bed velocities are relatively small and thus the eddy velocities and the corresponding sand concentration in the eddy are also relatively small. Thus, near the bed, there is a process of relatively large concentrations transported by relatively small velocities against the wave direction and a process of relatively small concentrations transported in the wave direction by relatively large velocities. Quantitative estimates of both processes indicate a net wave-related transport against the wave direction in case of a following current (Nap and Van Kampen 1988).

Finally, the importance of the wave-related transport $q_{t,w}$ in or against the current direction is discussed. Although only three experiments were carried out, the wave-related transport seems to be of less importance for $\bar{U}_s/\bar{u} < 2$. Neglecting the $q_{t,w}$ component with respect to the $q_{t,c}$ component results in a systematic error of about 30%.

COMPARISON OF MEASURED AND COMPUTED TRANSPORT RATES

Applied Formulas

The following three methods were applied to compute the current-related suspended-transport rates: the Bijker (1971) method, the Nielsen (1985) method, and the Van Rijn (1985, 1989) method. These methods are all based on the computation of a time-averaged concentration and velocity

profile. The b -coefficient of Bijker formula, originally proposed to be $b = 5$ (Bijker 1971) for longshore transport, was used as a calibration parameter in this study (nonbreaking waves). A value of $b = 1$ yielded the best overall results. Since random waves were generated in the flume tests, a characteristic wave height and period must be defined to represent the wave spectrum. The methods of Bijker and Nielsen were originally developed for regular waves. Therefore, a probabilistic method based on the assumption of Rayleigh-distributed wave heights was applied. The transport rates were computed for individual wave heights and then multiplied (weighted) by the probability of occurrence of each wave height class. The method of Van Rijn (1985, 1989) has been developed for irregular waves applying the significant wave height and the peak period.

All three methods are sensitive to the bed roughness value k_s . Analysis of the experimental data shows k_s values up to 7 times the ripple height Δ_r . Therefore, transport computations were carried out for k_s values in this latter range. The k_s values giving the best agreement between measured and computed transport rates (Figs. 9 and 10) are

- Bijker: k_s is approximately $3\Delta_r$ for the $100\ \mu\text{m}$ sediment and approx. $1\Delta_r$ for the $200\ \mu\text{m}$ sediment.
- Nielsen: k_s is approximately $3\Delta_r$ for the $100\ \mu\text{m}$ sediment and approx. $1\Delta_r$ for the $200\ \mu\text{m}$ sediment.
- Van Rijn: k_s is approximately $3\Delta_r$ for the $100\ \mu\text{m}$ sediment and the $200\ \mu\text{m}$ sediment.

Results

Measured and computed current-related suspended transport rates $q_{s,c}$ according to the three methods are presented in Figs. 9 and 10.

The Bijker method overestimates (factor of 3 to 5) the transport rates in case of a weak current (0.1 and 0.2 m/s) and underestimates (factor of 3)

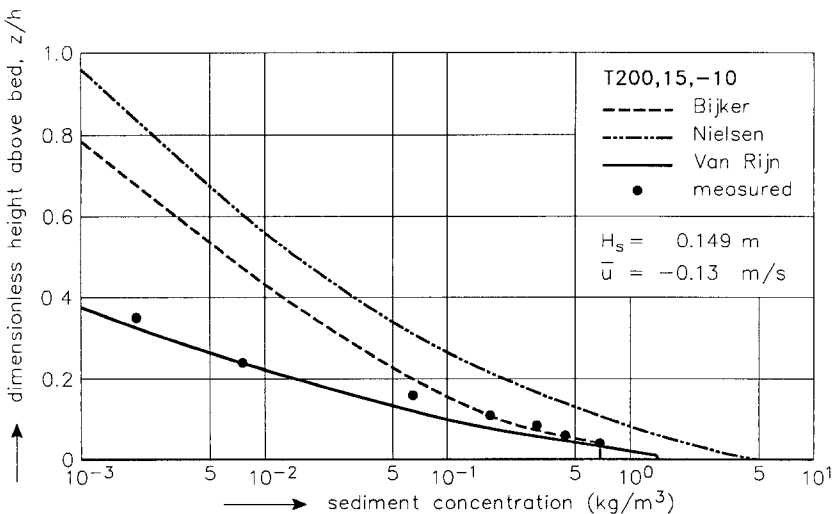


FIG. 15. Measured and Computed Concentration Profiles (T200,15,-10)

the transport rates in case of a strong current (0.4 m/s) for both the 100 μm and the 200 μm sediment. About 48% of the predicted transport rates are within a factor of 2 of the measured values. The discrepancies are mainly related to the computation of the sediment concentration profile. Figs. 11–16 show measured and computed concentration profiles. For a weak current (0.1), the concentrations are largely overestimated in the major part of the water depth. The predicted near-bed concentration is somewhat too small for the 100 μm sediment, but shows good agreement for the 200 μm sediment. For a relatively strong current (0.4 m/s), the shape of the concentration profile is much better represented, but now the predicted near-bed concentrations are much too small, resulting in an underprediction of the transport rates (Figs. 12, 14, and 16). Based on these results, it is concluded that the parabolic mixing coefficient distribution applied by Bijker is not correct for the combination of waves and a weak current, whereas the bed concentration prediction is not correct when a strong current is present.

The Nielsen method overestimates (factor of 5 to 10) the transport rates for the 200 μm sediment, mainly because the predicted concentrations are too large near the bed (weak currents 0.1, 0.2 m/s) and in the upper part of the water column (Figs. 15 and 16). The transport rates are also over-predicted (factor 5 to 10) for the 100 μm sediment in case of a strong current (0.4 m/s). This large overprediction cannot be explained from the predicted concentration profiles (Figs. 12 and 14), which show reasonable agreement in the near-bed region. The approximation function for the computation of the transport rates proposed by Nielsen is possibly not correct for fine sand (100 μm) in a strong current. Closer agreement between measured and computed transport rates would have been obtained by numerical integration of the concentration and velocity profiles instead of using the approximation function. Finally, it is noted that the Nielsen method is quite sensitive to the particle size of the bed material.

The Van Rijn method shows reasonable results over the full range of conditions. About 73% of the predicted transport rates are within a factor

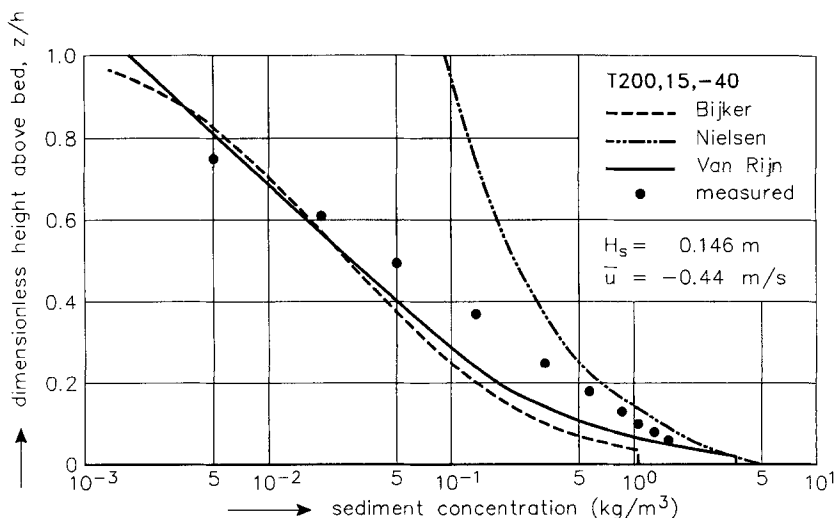


FIG. 16. Measured and Computed Concentration Profiles (T200,15,-40)

of 2 of the measured values. The computed concentrations show good agreement in the near-bed region both for the 100 μm and the 200 μm sediment. The concentrations in the upper layers are reasonably well predicted, with exception of the tests with large waves ($H_s = 0.18$ m) over a bed of 100 μm sediment (Figs. 13 and 14).

CONCLUSIONS

The main findings of this study can be summarized as follows:

The generation of waves in following or opposing currents causes a decrease of the time-averaged velocities in the near-bed region ($z/h < 0.2$). This effect increases for a larger wave height and is most pronounced for an opposing current. The waves cause a decrease of the near-surface velocities for a following current and an increase of the near-surface velocities in case of an opposing current.

A larger wave height leads to larger concentrations and to a steeper (more uniform) concentration profile, probably as a result of an increase of the wave-related mixing.

A weak current superimposed on the waves hardly affects the concentration profile. A strong current increases both the concentrations in the near-bed region and in the upper layer. The influence of the current direction (following or opposing) on the concentration profile is negligible.

The physical bed roughness height was found to be 3 to 7 times the ripple height.

The current-related transport rate varies with H_s^5 for a weak current and with H_s^2 for a strong current. The transport rate varies with $(\bar{u})^4$ for low waves and with $(\bar{u})^{2.5}$ for high waves. The transport rate shows a decrease by a factor of 3 to 6 for an increase of sediment size from 100 μm to 200 μm .

The magnitude of the wave-related transport rate is much smaller than the current-related transport rate ($q_{t,w}/q_{t,c} < 0.3$) for a ratio $\bar{U}_s/\bar{u} < 2$. The wave-related transport was found to be against the wave and current direction in some tests.

Comparisons of measured and predicted transport rates based on the methods of Bijker, Nielsen, and Van Rijn were performed. The Bijker method overestimates the transport rate for a weak current, but underestimates the transport rate for a strong current. The method of Nielsen shows discrepancies (factor of 5 to 10) for the 200 μm sediment and for the 100 μm sediment combined with a strong current. The method of van Rijn shows reasonably good results over the full range of conditions.

ACKNOWLEDGMENTS

The Delft University of Technology is gratefully acknowledged for providing flume facilities to perform a detailed study of the sediment transport process.

APPENDIX. REFERENCES

- Bijker, E. W. (1971). "Longshore transport computations." *J. Watrwy., Harb., and Coast., Engrg.*, 97(4), 687-703.
- Bosman, J. J. (1982). "Concentration distributions under waves and currents." *Rep. M1875*, Delft Hydraulics, Delft, The Netherlands (in Dutch).
- Bosman, J. J., and Steetzel, H. J. (1986). "Time and bed averaged concentrations under waves." *Proc., Coastal Engrg. Conf.*, Taiwan, 986-1001.

- Bosman, J. J., van der Velden, E., and Hulsbergen, C. H. (1987). "Sediment concentration measurements by transverse suction." *Coast. Engrg.*, 12, 353-371.
- Harms, J. C. (1969). "Hydraulic significance of some sand ripples." *Geol. Soc. Am. Bull.*, 80.
- Inman, D. L., and Bowen, A. J. (1963). "Flume experiments on sand transport by waves and currents." *Proc., 8th Coastal Engrg. Conf.*, Lisbon, 137-150.
- Jaffe, B. E., Sternberg, R. W., and Sallenger, A. H. (1984). "The role of suspended sediment in shore-normal beach profile changes." *Proc., Coast. Engrg., Conf.*, Houston, Tex., 1983-1997.
- Jonsson, I. G., Skougaard, C. H., and Wang, J. A. (1970). "Interaction between waves and currents." *Proc., Coast. Engrg. Conf.*, 489-508.
- Kemp, P. H., and Simons, R. R. (1982). "The interaction between waves and a turbulent current: Waves propagating with the current." *J. Fluid Mech.*, 116, 227-251.
- Kemp, P. H., and Simons, R. R. (1983). "The interaction between waves and a turbulent current: Waves propagating against the current." *J. Fluid Mech.*, 130, 73-91.
- Nap, E., and Van Kampen, A. (1988). *Sediment concentrations and transport in case of irregular non-breaking waves with a current, part A and B*. Dept. of Coast. Engrg., Tech. Univ. of Delft, Delft, The Netherlands.
- Nielsen, P. (1985). "Short manual of coastal bottom boundary layers and sediment transport." *Rep. TM85/1*, Public Works Dept., Sydney, Australia.
- Osborne, P. D., and Greenwood, B. (1992). "Frequency-dependent cross-shore suspended sediment transport, part 1 and 2." *Marine Geol.*, 106, 1-51.
- Quick, M. C. (1983). "Sediment transport by waves and currents." *Can. J. Civ. Engrg.*, 10(7), 142-149.
- Van der Kaaij, T. H., and Nieuwjaar, M. W. C. (1987). *Sediment concentrations and transport in case of irregular non-breaking waves with a current, part A and B*. Dept. of Coast. Engrg., Tech. Univ. of Delft, Delft, The Netherlands.
- Van Rijn, L. C. (1989). "Handbook of sediment transport in current and waves." *Rep. H461*, Delft Hydraulics, Delft, The Netherlands.
- Van Rijn, L. C. (1985). "Two-dimensional vertical mathematical model for suspended sediment transport by currents and waves." *Rep. S488 part IV*, Delft Hydraulics, Delft, The Netherlands.
- Van Rijn, L. C. (1990). *Principles of fluid flow and surface waves in rivers, estuaries, seas and oceans*. Aqua Publications, Amsterdam, The Netherlands.